Catalysis Science & Technology

Accepted Manuscript

ROYAL SOCIETY OF CHEMISTRY

www.rsc.org/catalysis

Catalysis Science & Technology RSCPublishing

ARTICLE

Hyperpolarisation through reversible interactions with *para*hydrogen

Cite this: DOI: 10.1039/x0xx00000x

Received 00th January 2012,
Accepted 00th January 2012

DOI: 10.1039/x0xx00000x

www.rsc.org/

Lyrelle S. Lloyd[a], Aziz Asghar[b], Michael J. Burns[a], Adrian Charlton[c], Steven Coombes[d], Michael J. Cowley[a], Gordon J. Dear[e], Simon B. Duckett[a], Georgi R. Genov[a], Gary G. R. Green[a], Louise A. R. Highton[a], Alexander J. J. Hooper[a], Majid Khan[a], Iman G. Khazal[a], Richard. J. Lewis[f], Ryan E. Mewis[a], Andrew D. Roberts[e] and Amy J. Ruddlesden.[a]

We describe here how the complexes Ir(COD)(NHC)Cl [NHC = IMes, SIMes, IPr, SIPr, ICy, IMe and $ImMe_2NPr^i_2$] provide significant insight into the catalytic process that underpins the hyperpolarization method signal amplification by reversible exchange (SABRE). These complexes react with pyridine and H_2 to produce $[Ir(H)_2(NHC)(py)_3]Cl$ which undergo ligand exchange on a timescale commensurate with good catalytic activity for the signal amplification by reversible exchange effect. This activity results from hydride ligand magnetic inequivalence and is highly dependent on the NHC. Variable temperature and kinetic studies demonstrate that rates of ligand loss which lie between 0.1 and 0.5 s^{-1} are ideal for catalysis. A role for the solvent complex $[Ir(H)_2(MeOH)(NHC)(py)_2]Cl$, which contains chemically inequivalent hydride ligands is revealed in the ligand exchange pathway. By optimisation of the conditions and NHC, a 5500-fold total pyridine signal enhancement is revealed when the NHC is IMes. Both T_1-reduction effects and HD exchange with the solvent are probed and shown to link to catalyst efficiency. The resulting signal enhancements suggest future *in-vivo* MRI measurements under physiological conditions using this catalytic effect will be possible.

Introduction

Nuclear Magnetic Resonance (NMR) spectroscopy is an important tool that is used widely to characterise molecules and probe their reactivity. Not withstanding this, it is an inherently insensitive technique because of the small nuclear spin-state population difference that exists between the energy levels it interrogates. For example, when proton nuclei are probed in a magnetic field of 9.4 T, they yield a ^{1}H NMR signal that is derived from effectively just 1 in every 32,000 of the proton nuclei present. One proven route to overcome this challenge is to drive the Boltzmann spin state population away this equilibrium position. This process corresponds to the creation of a hyperpolarized state, and when they are monitored prior to relaxation the detection of magnetic resonance signals of enhanced intensity results.

Hyperpolarized magnetic states have been produced by a variety of methods.[1-4] These include optical pumping which delivers hyperpolarized ^{129}Xe, ^{3}He and ^{83}Kr gases for further study.[5-7] The approach of Dynamic Nuclear Polarization (DNP) finds wider use owing to its commercialisation and delivers over 10,000-fold signal enhancements to a range of ^{13}C nuclei.[8, 9] Developments are targeting the application of this approach in human imaging.[10-12] Here we describe a series of results that employ *para*hydrogen (p-H_2)[13] in the creation of non-equilibrium spin order.[14] This approach has been referred to as PASADENA (*para*hydrogen and synthesis allow dramatically enhanced nuclear alignment)[15] and ALTADENA (adiabatic longitudinal transport and dissociation engenders net alignment)[16] with the term PHIP (*para*hydrogen induced polarization) being used to reflect both situations.[17] In these approaches, it is actually the product of a chemical reaction that incorporates two hydrogen atoms from a single p-H_2 molecule which is detected and significant mechanistic insight can be gained.[18-21] An effect, known as one-proton-PHIP,[22] has also been described by Eisenberg that has provided substantial mechanistic insight in which a single proton derived from p-H_2 provides hyperpolarization.[23-25] In 2008, the successful magnetization transfer from p-H_2 into a substrate was shown to be possible without the need for its chemical modification.[26] This new process was termed SABRE (signal amplification by

reversible exchange) to differentiate it from the earlier methods although the effect is manifest most readily in low-field and hence relates to ALTADENA.[27] This difference in nomenclature highlights the fact that whilst still utilising the non-equilibrium spin order of the *p*-H_2 singlet state to perturb a Boltzmann spin distribution, it achieves this in a chemically-unchanged target molecule which is different to the methods pioneered by Bowers *et al*.[15] and Eisenberg *et. al*.[17]

Although polarization transfer in SABRE is mediated by an inorganic catalyst their role is simply to enable the temporary formation of a scalar-coupled network between the hydride ligands on the catalyst and the nuclei of interest in the molecule that is targeted for hyperpolarization. During this period, the *p*-H_2 spin-order is shared with the ligated form of what will eventually become the chemically unmodified, and subsequently hyperpolarized substrate. Polarization transfer proceeds on the timescale of seconds and a growing range of molecules have been examined such as pyridine,[27] nicotinamide,[27, 28] isoniazid,[29] pyrazoles[30] and acetonitrile.[31] Such hyperpolarization would only be possible using conventional hydrogenative PHIP if a dehydro-form of the molecule were to exist, which can then be subject to the pairwise addition of H_2.[32-34] SABRE is therefore a catalytic effect involing the transfer of magnetism rather than chemical identity.

SABRE was first exemplified[26] using Crabtree's catalyst[35, 36] $[Ir(COD)(PCy_3)(py)][BF_4]$ (where COD is cyclooctadiene, py is pyridine and Cy is cyclohexyl). When this complex reacts with two equivalents of pyridine and H_2 it forms $[Ir(H)_2(PCy_3)(py)_3][BF_4]$ the active SABRE catalyst. Thus when this reaction is completed using *p*-H_2, transfer of its non-equilibrium nuclear spin order into the NMR-active nuclei of free pyridine results after ligand exchange.[37] This led to the observation of signal enhancements in the resulting ^1H, ^{13}C and ^{15}N NMR spectra of greater than 100-fold which translates into a 10,000-fold reduction in scan time when compared to routine NMR methods. Notably this signal gain is delivered after just a few seconds of exposure to *p*-H_2.

The magnetization sharing proceeds when the magnetic interactions in the complex match those required for transfer under strong coupling conditions.[38] As these interactions vary with magnetic field, the efficiency of transfer also varies with the field experienced by the sample at the time of catalysis. This behavior adds selectivity to the polarization transfer pathway and can be utilized to either enhance the resonances of specific sites in the target, or indeed, to control the type of magnetic state that is created.

A range of successful applications have been reported for SABRE which include the demonstration that the associated sensitivity gain facilitates trace component detection in low field.[39] The continuous low-field polarization of a bolus has also proven possible provided that a constant supply of *p*-H_2 remains available to the system in an analogous way to that of continuous monitoring through PASADENA in high field.[40] The recording of highly informative 1D- and 2D-NMR spectra that are diagnostic of the SABRE-target has enabled the detailed characterization of both reaction intermediates[31] and organic molecules in low concentrations at high field.[41,42] While the detection of reaction intermediates using PHIP reflects one of its major successes this area is currently less well developed for use with SABRE.[22, 43-46]

It has also been shown that when $[Ir(H)_2(PR_3)(py)_3][BF_4]$ was prepared *in-situ* by the simple addition of an appropriate phosphine to $[Ir(COD)(py)_2]BF_4$, the resulting complexes can be rapidly screened to identify an optimized catalyst.[37] The phosphine ligands employed in this study were PCy_3, $PPhCy_2$, PPh_2Cy, PEt_3, P^iPr_3, P^nBu_3, P^tBu_3 and P(1-naphthyl)$_3$ with $PPhCy_2$ presenting the highest activity. This further illustrates the catalytic concept behind SABRE and confirms optimization through ligand design is possible. As a start to this process, it has been reported that even greater SABRE efficiencies result when PR_3 is replaced by a more strongly electron-donating *N*-heterocyclic carbene (NHC) ligand.[47] For a number of years we have sought to extend our understanding of these carbene systems, and others have followed the same route.[48]

In this study we seek to add to these communications by examining the readily available N-heterocyclic carbene systems IMes (1,3-bis(2,4,6-trimethyl phenyl)imidazole, see SI for other definitions), SIMes, IPr, SIPr, ICy, IMe and $ImMe_2NPr^i_2$ (we refer to these collectively as **NHC** in this paper). The skeletal formulae of each of these ligands, which differ in their absolute

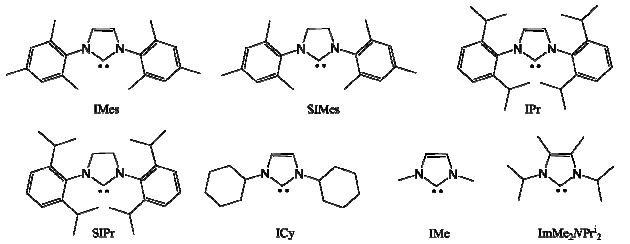

Figure 1 Carbene ligands, IMes, SIMes, IPr, SIPr, ICy, IMe and $ImMe_2NPr^i_2$, used in this study

electron donation power and their steric bulk are shown in Figure 1. Such effects are commonly assessed through buried volume[49, 50] and Tolman Electronic Parameter (TEP) values.[51] Thus when the ligand IMes is compared to SIMes the change in backbone causes the ligand to occupy more space around the metal centre. This is reflected in the buried volumes for [(IMes)Ir(COD)Cl][52] and [(SIMes)Ir(COD)Cl] increasing from 33.0% to 34.5%, respectively.[49] In order to separate the electronic and steric effects we have also included the IMe, IPr and SIPr analogues in this study. Now the NHC buried volumes are 26.3%, 34.9% and 35.4% respectively. Conversely, $ImMe_2NPr^i_2$ was used to increase the electron donating character of the system whilst retaining a relatively small buried volume ($\%V_{burr}$ = 38.4%). Of these carbenes, IMe is recognized as the weakest σ donor whilst ICy and $ImMe_2NPr^i_2$ are the strongest.

We link the results presented here to our earlier theoretical description of SABRE to suggest how utilization of these effect can be further improved.[38] We also seek to detail the complexity of the catalytic mechanism which underpins

SABRE in these systems in order to enable a fuller insight into the process to be shared with the scientific community.

Results and Discussion

The complexes [Ir(COD)(NHC)(Cl)] (**1-NHC**) [NHC = IMes, SIMes, IPr, SIPr, ICy, IMe and $ImMe_2NPr^i_2$] were isolated and their reaction with pyridine and H_2 examined. In the case of **1-IMes**[47] the reaction proceeds via the rapid formation of **2-IMes** which subsequently converts into **3-IMes** as shown in Scheme 1. As a consequence of this reaction we are able to produce a SABRE active complex through a reaction which involves an air-stable precursor which would be necessary if SABRE were to find wider use in MRI later.[28] In the absence of pyridine, the formation of highly reactive iridium trimers or C-H bond activation products result from such reactions with H_2.[53, 54]

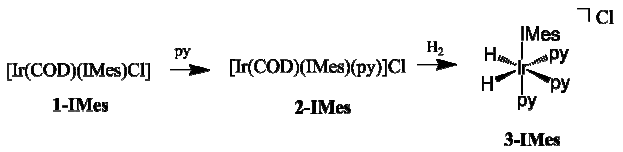

Scheme 1 Products from the reaction of [Ir(COD)(IMes)]Cl, (**1-IMes**) with H_2 and pyridine

This reaction is not limited to just **1-IMes**, and upon exposure of H_2 and pyridine to methanol-d_4 solutions of **1-NHC**, **3-NHC** forms as the dominant product in each case. Understanding this speciation is critical for SABRE as catalytic activity follows from the breaking of the magnetic symmetry of the two hydrogen nuclei which originate from *p*-H_2.[38] For **3-NHC**, activity results from the second order effect, magnetic inequivalence, although chemical inequivalence has been employed in other systems.[31]

In Table 1 we present the hydride chemical shifts, and specific ^1H, ^{13}C and ^{15}N chemical shifts of the carbene and pyridine ligands of **3-NHC**. They are listed in order of the decreasing electron-donating ability of the associated NHC, based on TEP data.[55] It might be reasonably expected that these chemical shift values should relate to the ligating power of the iridium centre. Table 1 reveals that whilst the hydride ligands chemical shifts move generally to higher field as the electron-donating power of the NHC ligand falls, the trend is not fully inline with the reported TEP data. This variation is also reflected in the Ir=^{13}C and Ir=C-^{15}N chemical shifts and the effects of the introduction of carbene backbone saturation are substantial. It has been reported previously that the change in ^{15}N chemical shift associated with pyridine binding Δδ (free-bound) relate to the extent of ligand interaction with a metal.[56] We present these data as the ^{15}N chemical shift of the ligand because we are dealing with a common reference point, and they reveal a larger change for the axial rather than the equatorial ligand (orientation in Scheme 1) and hence suggest a stronger Ir-N bonding interaction. It has been proposed previously that the catalyst lifetime is a key parameter for SABRE efficiency.[38] This situation arises because it is the spin-spin interaction between the hydride ligand and polarization receptor which propagates transfer, and this interaction is destroyed by ligand-metal bond-rupture. The lifetime of this interaction should therefore be influenced by the NHC, and reflected in the Δδ (free-bound) for the ^{15}N signal of pyridine. The predicted order is:

3-IMes > 3-IPr > 3-SIMes > 3-SiPr > 3-ICy > 3-$ImMe_2NPr^i_2$ > 3-IMe

A more accurate measurement of the complex lifetime would come directly from the associated rates of ligand loss. In the case of **3-NHC** there are two key ligand loss parameters that

Table 1. Selected NMR chemical shift data for **3-NHC** in methanol-d_4 solution.

Complex	^1H /δ		^{13}C/δ		^{15}N/δ	^{15}N/δ
	Ir<u>H</u>	N-(C<u>H</u>)$_2$N	N-<u>C</u>C-N	Ir=<u>C</u>	Ir=C-<u>N</u>	equatorial, axial pyridine
3-$ImMe_2NPr^i_2$	−22.77	N/A	125.7	176.3	198.5	253.8, 242.7
3-ICy	−22.49	7.22	117.7	197.6	202.4	254.0, 236.3
3-IMes	−22.56	7.18	122.4	194	194.5	255.6, 239.1
3-IPr	−22.60	7.16	123.6	177.5	194.4	255.2, 238.9
3-SIMes	−22.69	3.90	50.4	208.6	136.1	254.7, 240.1
3-SiPr	−22.24	4.11	53.8	182.9	138.9	254.4, 239.2
3-IMe	−21.98	7.15	121.7	221.5	177.9	251.6, 236.7

Table 2. Electronic, steric and thermodynamic activation parameters relating to the **3-NHC** complexes described here. The buried volumes are based on those reported for an M-NHC bond length of 2.00 Å in [(NHC)AuCl]; * indicates data extrapolated via Eyring analysis

Catalyst		**3-SIMes**	**3-ICy**	**3-IPr**	**3-SiPr**	**3-$ImMe_2NPr^i_2$**	**3-IMes**	**3-IMe**
TEP / (cm^{-1})		2051.5	2049.6	2051.5	2052.2	2049.6	2050.7	2054.1
$V_{CO}(Ir)^{av}$ / (cm^{-1})		2024.6	2023.0	2023.9	2024.9	–	2023.1	–
Buried Volume, $\%V_{burr}$ / (%)		36.9	27.4	44.5	47.0	38.4	36.5	26.3
Hydride	Raw Rate / s^{-1} (300 K)	36*	0.2	23.5	358*	2.9	9	0.07
	$\Delta H^‡$ / kJ mol^{-1}	75 ± 0.2	89 ± 1	103 ± 4	86 ± 1	79 ± 1	79 ± 0.2	109 ± 1
	$\Delta S^‡$ / J K^{-1} mol^{-1}	40 ± 1	43 ± 2	134 ± 2	97 ± 2	34 ± 2	43 ± 1	102 ± 3
	$\Delta G^‡_{300}$ / kJ mol^{-1}	63 ± 0.02	76 ± 0.02	64 ± 0.2	57 ± 0.04	69 ± 0.02	66 ± 0.02	79 ± 0.02
Pyridine	Raw Rate / s^{-1} (300 K)	45*	1.1	78.0	261*	14*	23	0.6
	$\Delta H^‡$ / kJ mol^{-1}	76 ± 1	94 ± 1	91 ± 1	82 ± 1	90 ± 1	95 ± 1	117 ± 3
	$\Delta S^‡$/ J K^{-1} mol^{-1}	45 ± 2	78 ± 4	99 ± 3	80 ± 1	83 ± 3	96 ± 2	148 ± 1
	$\Delta G^‡_{300}$ / kJ mol^{-1}	62 ± 0.05	71 ± 0.04	61 ± 0.02	58 ± 0.02	65 ± 0.06	66 ± 0.04	73 ± 0.05

are important, the rate constants for loss of pyridine and loss of H_2. The latter process is necessary for successful polarization transfer to take place..

For **3-IMes**, pyridine loss has been shown to be dissociative and independent of pyridine concentration.[47] It proceeds, therefore, via the formation of 16-electron $[Ir(H)_2(NHC)(py)_2]Cl$ which might itself be expected to rapidly form 18-electron $[Ir(H)_2(NHC)(methanol)(py)_2]Cl$ (**4-NHC**) in methanol (described later). Table 2 presents the rate constant data for pyridine and H_2 loss from **3-NHC** at 300 K, together with the NHC ligands' TEP values and buried volume terms. It also contains the associated activation parameters as determined by a series of variable-temperature measurements. Loss of the axial pyridine ligand in **3-NHC** is not observed in these studies in accordance with its stronger metal bonding interaction as detailed earlier. Such processes can, however, be complicated by competing associative and dissociative components.[57]

The presented pyridine loss rate constants reveal that all seven systems undergo ligand exchange on the timescale of seconds, and that the lifetimes of **3-NHC** vary with the NHC. The pyridine loss rate constants follow the order:

3-SiPr > 3-IPr > 3-SIMes > 3-IMes > 3-ImMe$_2$*N*Pr$^i_2$ > 3-ICy > 3-IMe

and hence the larger the NHC's buried volume, the faster the rate of pyridine loss. In fact, only **3-ImMe$_2$*N*Pr$^i_2$** lies outside this trend and hence steric effects impart significant control over this process.

It can be seen, from the $\Delta H^{\neq}$ data, that the associated Ir-py bond energies vary dramatically from 76 ± 0.4 to 117 ± 3 kJ mol^{-1} across this ligand series. While the associated $\Delta S^{\neq}$ terms are all positive, in agreement with a dissociative reaction, they show an even larger variation (148.0 ± 1.0 to 45.0 ± 1.5 J K mol^{-1}).

For **3-IMe**, the $\Delta S^{\neq}$ value is 148.0 ± 1.0 J K mol^{-1} while the $\Delta H^{\neq}$ value is 117.0 ± 3.0 kJ mol^{-1} and they are particularly notable. These values tell us that the least sterically-encumbered NHC results in both the largest Ir-py bond energy and the greatest release in entropy upon reaching the transition state for pyridine loss. In contrast for **3-SiPr**, the bulkiest NHC of the series, $\Delta S^{\neq}$ = 82 ± 1 J K mol^{-1} and $\Delta H^{\neq}$ = 80 ± 1 kJ mol^{-1}, and hence a smaller Ir-py bond energy (longer Ir-py bond) and a smaller release in entropy on reaching the transition state for ligand dissociation results.

Care needs to be taken when interpreting these data further because for **3-SIMes**, $\Delta S^{\neq}$ is 45 ± 2 J K mol^{-1} and $\Delta H^{\neq}$ is 76 ± 1 kJ mol^{-1}. This means that the complex with the weakest Ir-py bond energy of the series coincides with the smallest change in entropy on reaching the TS for pyridine loss. Thus even though **3-SIMes** and **3-IMes** are very similar in size, these parameters reveal very different reactivity due to what must now be an electronic effect. It is possible therefore to conclude that the resulting electronic stabilisation of the ground state, increases the Ir-py bond energy, thereby lowering the rate of pyridine loss. Furthermore, increasing the NHC's steric bulk offsets this change by pushing the pyridine ligand away from the metal centre and weakening the Ir-py bond whilst reducing the beneficial entropy change associated with ligand loss. The complexity in assessing the underlying ground and excited state contributions is, however, well established.[58] We can also see that the apparent Δδ (^{15}N-free-bound-(pyridine)) values do not match with these data.

The formation of the highly reactive solvent complex $[Ir(H)_2(NHC)(methanol)(py)_2]Cl$ (**4-NHC**) upon pyridine loss has also been demonstrated. This was achieved by examining a methanol-d_4 solution of **3-IMes** at 265 K where the ligand exchange processes are slowed. Now, a dominant hydride signal for **3-IMes** is seen in the corresponding ^{1}H NMR spectrum at δ -22.56, alongside two further very weak hydride signals at δ -23.44 and δ -25.49. The relative integrals of these signals suggest that **3-IMes** and the new complex **4-IMes** are present in the ratio 100:1. Because of the equilibrium position, the complete characterisation of **4-IMes** by NMR is impractical. However, when a methanol-d_4 solution of **3-IMes** containing a 20-fold excess of pyridine is exposed to *p*-H_2 at 253 K the NMR signals for the hydride ligands of **4-IMes** show PHIP. These signals appear at 14% of the intensity of the hydride signal for **3-IMes** and share a common J_{HH} coupling of –10.51 Hz. Furthermore, only the δ –23.45 hydride signal exhibits a *trans* ^{15}N-hydride coupling of 15 Hz when this reaction is monitored with ^{15}N-labelled pyridine. In addition, we note that upon adding H_2O to this sample, the hydride signal of **4-IMes** at δ −25.49 moves to δ −25.74 due to the formation of $[Ir(H)_2(NHC)(H_2O)(py)_2]Cl$ thereby confirming that the hydride ligand giving rise to this signal is *trans* to methanol.[59-61]

The observation of the PHIP effect in the hydride resonances of **4-IMes** also confirms that there is a route to introduce protons from *p*-H_2 into it before relaxation takes place. This has implications for SABRE using **1-NHC** because the related complex $[Ir(H)_2(CH_3CN)(IMes)(PPh_3)(py)]BF_4$ is an active catalyst.[31] Indeed, the low concentration of **4-IMes** does not necessarily preclude its importance since the field dependence associated with SABRE efficiency (see later) and the complexes lifetime in solution are important contributors to

Table 3 Methanol adducts, **4-NHC**, detected under PHIP conditions at 253 K. The hydride chemical shifts and the PHIP hydride signal intensity as a percentage of the hydride signal of **3-NHC** are listed.

NHC	Hydride signal (δ)			PHIP signal %
	3-NHC	**4-NHC**		
ImMe$_2$*N*Pr$^i_2$	−22.63	−22.56	−26.51	66
ICy	−22.39	−22.35	−26.00	60
IMes	−22.56	−23.44	−25.49	14
IPr	−22.60	−23.47	−25.51	22
SIMes	−22.55	−22.12	−27.47	0.7
SiPr	−22.24	Not seen	-	-
IMe	−22.02	−22.10	−25.69	31

its activity. Selectivity problems are a common feature of catalysis and illustrate why rigorous mechanistic study is necessary for reaction optimisation.[62]

Table 3 sets out the ratio of the PHIP enhanced hydride signal intensities seen for **4-NHC** relative to those of **3-NHC**, and their chemical shifts. We report these data in this way because the observation of the NMR signals for **4-NHC** using standard NMR methods proved to be impractical. The two most electron donating ligand systems, **ICy** and **ImMe$_2$*N*Pr$^i_2$** proved to yield the strongest PHIP enhanced hydride signals for **4-NHC**, when compared to those of **3-NHC**, whilst the bulkier but poor electron donating **SIPr** system was not observed to yield any detectable methanol-adduct. When the **ImMe$_2$*N*Pr$^i_2$** system was monitored at 253 K immediately after taking the sample out of the magnet, shaking the NMR tube containing normal H_2 and then returning it to the magnet, **4** initially proved to be visible at *ca*. 8% of the level relative to **3** but rapid equilibration led to an impractical <0.5% level when characterisation was attempted.

A reported theoretical studying using density functional theory has suggested that the H_2 exchange step proceeds via the formation of 18-electron $[Ir(H)_2(H_2)(NHC)(py)_2]Cl$.[47] This process is captured in the reaction pathway illustrated in Scheme 2 where the pyridine loss product $[Ir(H)_2(NHC)(py)_2]Cl$ is competitively trapped by methanol. This step has been confirmed experimentally at 265 K by probing the kinetic fate of the hydride ligands of both the major and minor hydride species in a series of long-acquisition time EXSY measurements under 3 atm. H_2 pressure. The modelling of these data revealed that the experimentally dominant H_2 loss pathway actually proceeds via **4-IMes,** with an observed rate of H_2 loss of 1.72 s^{-1}. Under these conditions, the rate of conversion of **3-IMes** into **4-IMes** proved to be 0.08 s^{-1} and the rate for **4-IMes** returning to **3-IMes** was 4.14 s^{-1}.

The successful trapping of what would be 16-electron $[Ir(H)_2(NHC)(py)_2]Cl$ by methanol and the subsequent involvement of **4-IMes** in the H_2 loss pathway reflects the fact that the concentration of methanol far exceeds that of H_2.

Further confirmation for this reaction pathway comes from the observed linear dependence of the H_2 loss rate with H_2 concentration over the H_2 pressure range 1 to 3 bar. H_2 loss is also inhibited by added pyridine in accordance with the associated shift in equilibrium towards **3-IMes**. The trend-line imposed gradient found in these H_2 concentration studies proved larger for SIMes than for IMes and ImMe$_2$*N*Pr$^i_2$ in agreement with its higher H_2 loss rate (Table 2).

The detection of these methanol adducts also provides insight into the observed H/D exchange processes that equilibrates the Ir-H and OD groups in these reactions. Experimentally this process is reflected in the formation of readily detected HD and $[Ir(H)(D)(NHC)(py)_2]Cl$ and $[Ir(D)_2(NHC)(py)_2]Cl$ during the course of this reaction. This process led to complications when the EXSY methods were used to follow the hydride ligand exchange pathway. We, employed CD_3OH to remove this effect but note that the formation of $[Ir(H)(D)(NHC)(py)_3]Cl$ leads to an isotopic

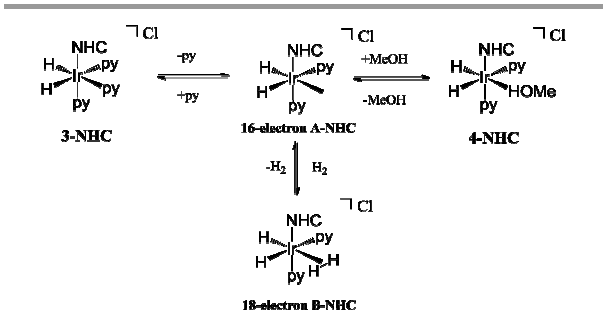

Scheme 2 Ligand exchange pathways for **3-NHC**

perturbation in the hydride ligands chemical shift when compared to that of $[Ir(H)_2(NHC)(py)_3]Cl$. This means that when a suitably selective shaped pulse is applied and slower rates of exchange operate H_2 and HD elimination rates can be distinguished.

Considering the role of such HD exchange processes during catalysis is important because it provides an additional route to reduce the SABRE effect. It does this by reducing the catalyst lifetime and promoting 1-proton PHIP.[24, 63, 64] Both of these processes correspond in a classical sense to catalyst deactivation. We determined the rates of IrD formation in these systems through transfer from MeOD at 298 K. For **3-SIMes** the rate was 0.06 x10^{-4} s^{-1}, whilst for **3-IPr** it was 0.7 x10^{-4} s^{-1} and for **3-IMes** it was 1.2 x10^{-4} s^{-1}. Hence these rates of reaction are too slow in this case to interfere with SABRE. We have also assessed the rate of deuterium incorporation in pyridine, and note that this process was reported as being too slow to interfere with the SABRE measurements in the case of PCy_3.[65] A recent paper has, however, described how the introduction of a single proton from *p*-H_2 into the *ortho* proton of pyridine via a CD bond activation reaction led to what we suggest is one-proton PHIP in the pyridine-d_4-H signal.[66] When pyridine-d_5 (99.5%, Aldrich) was used in this study, substantial SABRE polarisation of the ^{1}H nuclei in residual pyridine-d_4-H was observed across all 3 sites under transfer at 65 G. In this case, the order of overall signal enhancement proved to be IMes > SIMes~IPr, although the site specific relative intensity gain was approximately 87 % (*ortho*), 10 % (*para*) and 3 % (*meta*). When a measurement was repeated 2 mins after sample introduction in order to limit the SABRE effect, the *ortho* proton pyridine site alone showed emission character. Its intensity in this measurement was just 0.3 % of that seen under SABRE for IPr, 0.13 % for IMes and 0.23 % for SIMes. While these data are further complicated, by the long proton relaxation times of the pyridine-d_4-H isotopomers, it would, therefore, appear that such effects are relatively small in size.

One further aspect that needs to be considered is that of magnetic spin state relaxation. When **3-NHC** is acting as the polarisation transfer catalyst (as described later) it does so by redistributing magnetisation at a molecular level. This is an equilibrium process that operates in both directions and hence might also be expected to be visible as an enhanced rate of signal relaxation. The role of **3-NHC** on the relaxation of the

proton spins in pyridine was, therefore, quantified. For control purposes, the T_1 relaxation times for the *ortho*, *meta* and *para* protons of pyridine were measured as 27.8, 27.7 and 36.5 s respectively under dinitrogen, and 24.9, 24.5 and 29.3 s respectively in air. Table 4 lists the corresponding T_1 values of the three sites of pyridine, determined for a series of test samples where its concentration was 100 mM and the original **1-NHC** catalyst loading was 5 mol%. The T_1 values were determined in the presence of the catalyst, and with, and without, H_2 gas. It is clear from these data that the T_1's are substantially affected by the presence of both **1-NHC** (it forms **2-NHC** in the absence of H_2) and **3-NHC** in solution. Table 4 also lists the lifetime of **3-NHC** according to the data of Table 2 (lifetime is the reciprocal of twice the listed rate constant).

For **1-ICy**, **1-ImMe$_2$*N*Pr$^i_2$**, and **1-IMe** there is a dramatic

Table 4 T_1 values at 298 K for the indicated pyridine resonances in presence of **1-NHC** or **3-NHC** and H_2 as indicated.

NHC/ pyridine proton	**1-NHC**			3 bar H_2 and **3-NHC**			lifetime /s
	ortho	*meta*	*para*	*ortho*	*meta*	*para*	
IMes	28.8	26.4	30.1	12.6	14.7	18.9	0.022
IPr	30.5	26.3	35.2	13.3	15.5	20.6	0.006
SiPr	31.1	27.2	36.1	14.4	14.5	18.8	0.0019
SIMes	32.5	27.8	35.0	15.9	18.0	23.1	0.011
ICy	16.4	19.2	24.2	17.2	17.9	22.9	0.45
ImMe$_2$*N*Pr$^i_2$	18.7	19.1	23.9	20.1	20.9	25.6	0.035
IMe	22.3	21.5	28.0	22.9	20.0	26.6	0.83

increase in relaxation efficiency associated with the formation of **2-NHC**, and the reversible binding of pyridine to it. The formation of **3-NHC** also dramatically assists pyridine relaxation with the largest % change being seen for the **SiPr** and **IMes** systems; the longer lived complexes show a reduced effect. The presence of the catalyst in solution will therefore acts to reduce the steady-state level of hyperpolarisation that can be observable through SABRE because it takes several seconds for the sample to move from position where polarization transfer takes place into the final position where high-field measurement can take place. It is therefore highly desirable to remove the catalyst prior to measurement.

Investigation of the SABRE effect. In order to explore the catalytic effect of SABRE and make use of the observations described earlier, a series of methanol-d_4 samples with a pyridine and **1-NHC** were placed under 3 atm. of *p*-H_2. These samples were prepared in 5 mm NMR tubes and shaken for 10 seconds prior to transferring them into the spectrometer for observation. A typical NMR spectrum obtained in this way is shown in Figure 2; hyperpolarised signals in emission mode are seen for the three resonances of free pyridine. Furthermore, three smaller peaks for bound equatorial pyridine ligands are observed in these spectra which also possess emission character. Figure 3 reveals the associated sum of the signal enhancement levels for the 3 separate pyridine proton sites as determined in such an experiment over the temperature range 215 K to 335 K. It can clearly be seen from these data that **3-IMes** reflects the optimal polarisation system under these conditions. Furthermore, **3-IPr** and **3-SIMes** perform well. The performance of the remaining systems is much worse, with **3-ImMe$_2$NPr$^i_2$** > **3-IMe** > **3-ICy** > **3-SIPr** at 290 K.

Two enhancement trends are revealed in this variable temperature study. The first trend is readily visible for the **3-ICy** or **3-IMe** systems where hyperpolarisation efficiency proves to increase with increase in temperature. In the case of **3-IMe**, the rate constant for pyridine loss (per pyridine ligand) is 0.6 s^{-1} at 300 K whilst for **3- ICy** it is 1.3 s^{-1}. This suggests

Figure 2 ^{1}H NMR spectra of pyridine (0.1 M) of a fully relaxed sample (A) and after hyperpolarisation transfer at -65 G in the presence of **3-IMes** and *para*hydrogen (B). The top trace has been enlarged by a factor of 64 fold relative to the bottom trace.

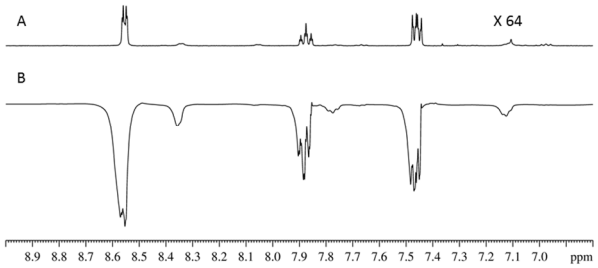

that their lifetimes are too long at 300 K for optimal magnetisation transfer, and hence that increasing the temperature, thereby increasing the rate of ligand exchange,

Figure 3 Effect of temperature on the total signal enhancement seen for pyridine when hyperpolarised using the indicated **3-NHC.**

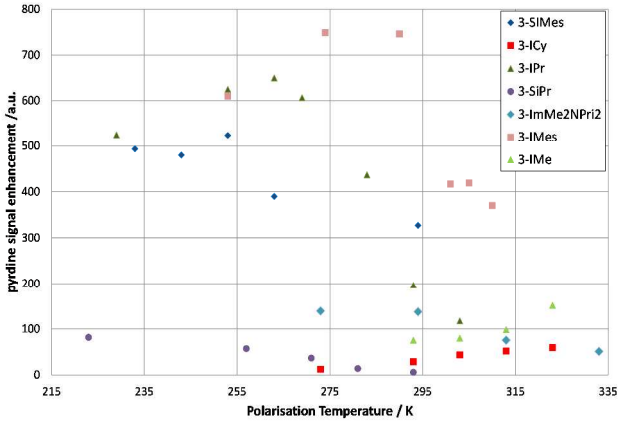

promotes SABRE. In contrast for **3-SiPr** the pyridine loss rate is 261 s^{-1} at 300 K and is now too high for efficient transfer; cooling improves SABRE efficiency.

The best hyperpolarisation system under these conditions resulted from **3-IMes**. Now a curve with a local maximum is observed such that at 274 K the rate of pyridine loss is 0.25 s^{-1}. For **3-IPr** better activity is found at *ca*. 253 K where the corresponding ligand exchange rate is 0.04 s^{-1}, and for **3-SIMes** 253 K again yields an optimal enhancement where the corresponding rate constant is 0.07 s^{-1}. These observations

confirm that the optimum rate of pyridine exchange per mole of complex lies between 0.5 and 0.08 s^{-1}.

The corresponding rate constants for H_2 loss for the IMes, SIMes and IPr systems are 0.34 s^{-1} (274 K), 0.11 s^{-1} (253 K) and 0.01 s^{-1} (253 K). This is consistent with the higher H_2 exchange rate of IMes increasing its SABRE activity relative to the others.

Magnetic field effects. Using a purpose-built apparatus designed by Bruker and the University of York, we have completed a range of measurements to expand our understanding of the SABRE effect by reference to these systems.[47] This apparatus allows the polarisation/repolarisation of samples via an external reaction cell in conjunction with a flow probe for NMR measurement. The *p*-H_2 that is employed in this study is produced by cooling to 30 K. The magnetic field experienced by the sample at the point of polarization transfer controlled via a copper coil which surrounds it. This coil can be used to generate a defined magnetic field between -150 and +150 G that is aligned in the vertical direction. *p*-H_2 gas was bubbled through a series of solutions for 6 seconds prior to their transfer into the flow probe, a process which takes 3.9 s up to the point of measurement. The system was flushed and dried between runs to ensure that the concentrations of substrate and catalyst remained well defined. The effect of changing the magnitude of the applied magnetic field during this process is exemplified in Figure 4 for the *para* proton of pyridine and **3-IPr**.

Figure 4 Effect of changing the magnitude of the magnetic field experienced by the sample polarisation at the point of polarisation transfer on the para proton signal intensity of pyridine using **3-IPr** as the catalyst.

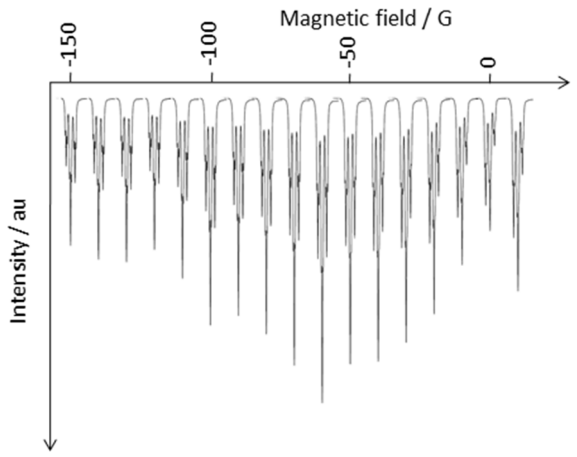

The effect of changing the polarisation transfer field (PTF) was investigated for each catalyst. Table 5 lists the magnetic field associated with maximum signal enhancement together with the associated enhancement values produced in this apparatus.

We note the values listed in Table 5 differ from those reported by van Weerdenburg *et al*[48] who used a 10 mM concentration of catalyst which significantly increases the enhancement observed with IMes (~700 fold) whilst diminishing it for ICy (~ 18 fold). Furthermore, as they note some cleaning solvent is left in the apparatus, the actual concentrations of catalyst and pyridine may be lower than quoted. A detailed comparison of these data is, therefore, not possible. Their reported field maxima, do occur in similar regions to those observed here, suggesting that this property is not affected significantly by concentration of the catalyst or substrate. It is, however, affected by the catalyst lifetime, moving to higher PTF as it falls.

Table 5 Polarisation transfer field values yielding the maximum signal gain for the specified NHC at 298 K. Catalysts are listed in terms of decreasing lifetime.

NHC	Field (G)	Observed pyridine proton signal enhancement and sum			
		ortho	*meta*	*para*	|Total|
IMe	-60	-1.7	-2	-0.6	4.1
$ImMe_2NPr^i_2$	-60	-113.6	-104.8	-64.0	500.6
ICy	-60	-8.4	-9.2	-4.8	40.1
SIMes	-90	-82.7	-102.7	-63.3	434.2
SiPr	-150	-15.4	-11.9	-16.0	70.6
IPr	-60	-17.1	-12.7	-19.6	79.2
IMes	-60	-165.4	51.0	70.2	503.0

Table 5 reveals that the three best room temperature catalysts of this series employ IMes, SIMes and IPr ligands. We have therefore investigated a range of parameters to further optimise their performance. The effects of the absolute concentrations of the catalysts and substrate were examined. Figure 5 portrays the effect of changing the catalyst concentration whilst keeping the pyridine to metal ratio constant at 20:1. It can be seen from these data that all three catalysts yield good levels of hyperpolarisation even at low concentration, although when the catalyst concentration is lower than 2.5 mM there is a fall in SABRE efficiency.

Figure 5 Effect of catalyst concentration (mM) on the total polarisation transfer level (signal enhancement) for a 17-fold pyridine excess and 5 mol % 1-NHC loading.

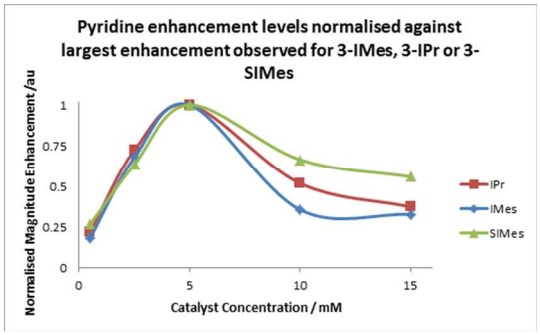

Figure 6 Effect of substrate to **3-NHC** excess on the level of polarisation transfer for a metal concentration of 5mM.

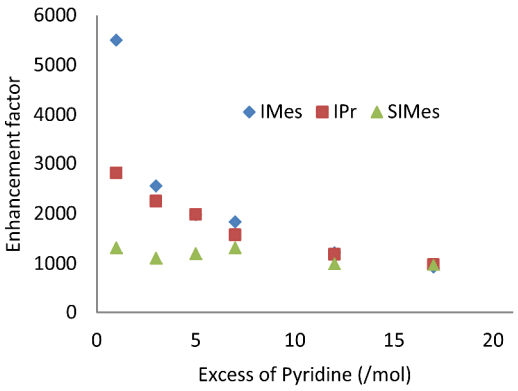

When a constant 5mM catalyst concentration is employed, and the level of pyridine excess relative to iridium changed from 1 to 200-fold the level of polarization proved to vary as shown in Figure 6. Now the IMes system delivers a total pyridine proton enhancement level of 5500-fold when the metal to pyridine ratio is 1:4. A further series of studies were undertaken with this optimised 1:4 catalyst to pyridine ratio where the metal concentration was varied and the largest enhancement was produced with a 5mM concentration (see supplementary).

Given the importance of H_2 in this process we have also tested the effect of H_2 pressure on the level of enhancement for the IMes system. These measurements employed a 5 mM metal concentration and were made over the pressure range 1 to 8 bar in both small volume medium and heavy walled 5 mm NMR tubes. The increase in H_2 pressure results in a non-linear response as shown in Figure 7 which plateaus at 8 bar and the enhancement level is affected by the mixing process.

Figure 7 Effect of *p*-H_2 pressure on the normalised level of polarisation transfer for **3-IMes** using heavy- and medium-walled tubes.

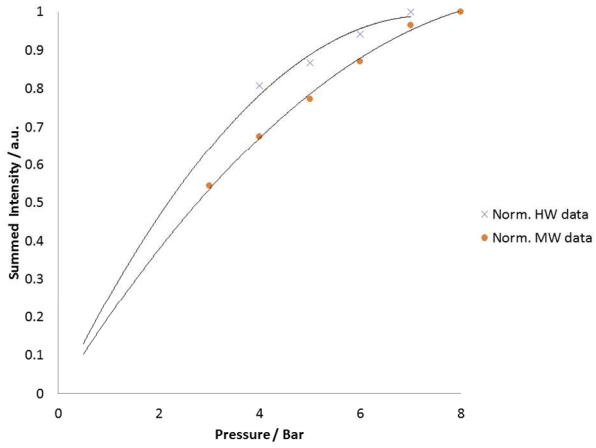

Extrapolation of the thin walled 5 mm NMR tubes 3 bar, 5500-fold enhancement to 8 bar is predicted to increase this value to ≈10,100. A number of groups have worked on assessing the detection threshold of SABRE.[39, 67, 68]

Conclusions

The challenges associated with using SABRE to generate non-Boltzmann spin state populations in organic substrates via *p*-H_2 have been illustrated. This hyperpolarization approach does not involve a formal hydrogenation step as is usual in PHIP but instead the substrate and *p*-H_2 are brought into temporary association through a transition metal complex. The sharing of spin polarization from the hydride ligands of this template with the substrate then takes place (the hyperpolarization target). This process is catalytic in nature even though it does not change the chemical identity of the target. Indeed, the catalyst acts to polarise multiple copies of the polarisation target in a process that can be optimised through a combination of ligand variation, reagent concentration change and temperature control. *p*-H_2 is the limiting reagent in these studies as it contains a specific amount of subsequently accessible polarisation per molecule. Consequently by changing the relative excess of this polarisation source with respect to the number of protons in the hyperpolarization target, improved efficiency can be achieved. This spin-order excess is directly controlled by the H_2 concentration, the substrate concentration and the substrate complexity, specified in terms of the number of protons (nuclei) available to accept the polarisation.

The catalyst effect is monitored through the complexes [Ir(COD)(NHC)(Cl)] (**1-NHC**) [NHC = IMes, SIMes, IPr, SIPr, ICy, IMe and $ImMe_2NPr^i_2$] which all react with pyridine and H_2 to form the active SABRE catalyst $[Ir(H)_2(NHC)(py)_3]Cl$ (**3-NHC**). Ligand exchange studies revealed that the loss of pyridine from **3-NHC** is dissociative and controlled by both the electronic and steric parameters of the NHC. When the NHC is bulky, it weakens the ground-state Ir-py interaction thereby promoting pyridine dissociation. A reduction in the release in entropy follows from this change which acts to counter the bond energy change, such that at 300 K,

3-SiPr > 3-IPr > 3-SIMes >3-IMes > 3-$ImMe_2NPr^i_2$ > 3-ICy > 3-IMe.

This dissociative process was shown to result in the ready detection of $[Ir(H)_2(NHC)(methanol)(py)_2]Cl$ (**4-NHC**) through PHIP. While **4-NHC** is SABRE active, in this case its low concentration results in a minimal role in hyperpolarising pyridine. This solvent complex, however, provides the dominant route to $[Ir(H_2)(H)_2(NHC)(py)_2]Cl$, a species that is directly involved in the process of H_2 exchange. The corresponding rates of H_2 loss, monitored via magnetization transfer from **3-NHC** were observed to follow the following trend,

3-SiPr > 3-SIMes > 3-IPr > 3-IMes > 3-ImMe$_2$*N*Pr$^i_2$ > 3-ICy > 3-IMe.

This chemical change follows the loss of pyridine from **3-NHC** and exhibits a linear dependence on H_2 concentration. Hence the intimate nature of both the H_2 loss and pyridine loss processes show significant and relatively similar steric and electronic effects. The short lifetimes of **4-NHC** suggest this species role in SABRE is minimal. Furthermore, hydrogen-deuterium exchange between the Ir-H and the solvent also interferes with the SABRE process. However, again only a minimal effect is evident. The replacement of an *ortho* pyridine proton with a proton from *p*-H_2 also leads to a weak signal enhancement that which is visible when pyridine-d_5 is used as the substrate.[66] Again, this process contributes minimally to the detected SABRE signals described earlier. The effect of these catalysts on the T_1 of the protons of pyridine has also been ranked:

3-IMe < 3-ImMe$_2$*N*Pr$^i_2$ < 3-ICy < 3-SIMes < 3-IPr < 3-SiPr < 3-IMes.

These values provide a direct estimate of the ability of **3-NHC** to influence the proton magnetisation associated with pyridine and thereby reflect their potential SABRE activity. The **3-IMes** complex produced the largest effect on the substrates proton T_1 values and it is the most effective SABRE catalyst at 300 K as revealed in the following order:

3-SiPr < 3-ICy < 3-IMe < 3-ImMe$_2$*N*Pr$^i_2$ < 3-SIMes < 3-IPr < 3-IMes.

The described variable temperature studies showed that the optimal pyridine ligand exchange rates lie between 0.04-0.25 s^{-1} (Figure 4, per mole of complex). This means that the optimum catalyst lifetime lies between 12.5 s and 2 s. We can also see from the variation in SABRE efficiency with polarisation transfer field that the optimum field value increases as the catalyst lifetime decreases (Table 5). When a 5mM **3-NHC** concentration was employed and the pyridine excess varied, for **3-IPr** and **3-IMes** the presence of a single equivalent of pyridine led to optimal hyperpolarization in accordance with the limiting reagent description used here. We have tested the effect of metal concentration at this ligand loading, producing a total pyridine signal enhancement of 2807 for **1-IPr**, 5500 for **1-IMes** and 1317 for **1-SIMes** at 5mM metal concentrations after transfer at 65 G. Such signal improvements are of great significance since the signal to noise ratio varies with the square of the number of observations. These measurements were completed in a 5 mm NMR tube under 3 atm. of H_2 gas. When a high pressure tube is employed, a non-linear dependence on the H_2 concentration is revealed up to a pressure of 8 bar, above which it tends to plateau. We can, therefore, conclude that if optimal H_2 mixing is possible, at 8 Bar of H_2 the 5500 fold enhancement would increase further to ≈10100. These values suggest that *in-vivo* detection in conjunction with SABRE will be possible in the future and reveal how such substrate/catalyst optimisation studies can be undertaken.

Acknowledgements
This work has involved a large team of researchers working on the various Ir-NHC systems. We therefore thank a number of sources for funding this work. These include the University of York, the Hull-York Medical School, a York based White Rose Healthcare Innovation Programme, the EPSRC (grant no. EP/G009546/1), the Wellcome Trust (092506 and 098335), Nuffield (URB/39689, AJR and GRG), Bruker Bio-Spin, the Spanish MEC (Project Consolider ORFEO (CSD 2007-00006)). We are also grateful to staff at Bruker BioSpin (especially Joost Lohman, Jean-Max Tyburn, Patrick Krencker and David Kilgour) and the University of York (Mark Mortimer, Anthony Atkin, Kevin Atkinson, Katharine Armour, Richard Green and Richard John) for helpful discussions. Astra-Zeneca, FERA and GlaxoSmithKline are also thanked. We thank, Paul I. I. Elliott (University of Huddersfield), Michael Bernstein and Christopher J. Sleigh of Astra-Zeneca for support.

Notes and references

[a]Centre for Hyperpolarization in Magnetic Resonance, University of York, York Science Park, York, YO10 5NY, U.K. email, simon.duckett@york.ac.uk.
[b]Hull York Medical School, University of Hull, Cottingham Road, Hull, HU6 7RX.
[c]The Food and Environment Research Agency, Sand Hutton, York, YO41 1LZ. UK.
[d]AstraZeneca R&D Pharmaceutical Development, Silk Road Business Park, Charter Way, Macclesfield, Cheshire. SK10 2NA, UK.
[e]GlaxoSmithKline Research & Development Limited, Park Road, Ware, Hertfordshire, SG12 0DP, UK.
[f]AstraZeneca R&D Mölndal, Respiratory & Inflammation Innovative Medicines, Pepparedsleden 1, S-431 83 Mölndal, Sweden.

Electronic Supplementary Information (ESI) available: sample preparation, signal enhancement methods and raw data. See DOI: 10.1039/b000000x/

1. D. Blazina, S. B. Duckett, J. P. Dunne and C. Godard, *Dalton Trans.*, 2004, 2601-2609.
2. S. B. Duckett and C. J. Sleigh, *Prog. Nucl. Magn. Reson. Spectrosc.*, 1999, **34**, 71-92.
3. S. B. Duckett and N. J. Wood, *Coord. Chem. Rev.*, 2008, **252**, 2278-2291.
4. K. Golman, L. E. Olsson, O. Axelsson, S. Mansson, M. Karlsson and J. S. Petersson, *Br. J. Radiol.*, 2003, **76**, S118.
5. Z. I. Cleveland, G. E. Pavlovskaya, N. D. Elkins, K. F. Stupic, J. E. Repine and T. Meersmann, *J. Magn. Reson.*, 2008, **195**, 232-237.
6. G. E. Santyr, W. W. Lam, J. M. Parra-Robles, T. M. Taves and A. V. Ouriadov, *J. Appl. Phys.*, 2009, **105**, 102004.
7. X. J. Xu, G. Norquay, S. R. Parnell, M. H. Deppe, S. Ajraoui, R. Hashoian, H. Marshall, P. D. Griffiths, J. Parra-Robles and J. M. Wild, *Mag. Res. Med.*, 2012, **68**, 1900-1904.

8. J. H. Ardenkjær-Larsen, B. Fridlund, A. Gram, G. Hansson, L. Hansson, M. H. Lerche, R. Servin, M. Thaning and K. Golman, *Pro, Nat. Acad. Sci.*, 2003, **100**, 10158-10163.
9. K. R. Keshari and D. M. Wilson, *Chem. Soc. Rev.*, 2014, **43**, 1627-1659.
10. S. J. Nelson, D. Vigneron, J. Kurhanewicz, A. Chen, R. Bok and R. Hurd, *Appl. Magn. Reson.*, 2008, **34**, 533-544.
11. I. Park, P. E. Z. Larson, J. L. Tropp, L. Carvajal, G. Reed, R. Bok, F. Robb, J. Bringas, A. Kells, P. Pivirotto, K. Bankiewicz, D. B. Vigneron and S. J. Nelson, *Mag. Res. Med.*, 2014, **71**, 19-25.
12. J. Kurhanewicz, D. B. Vigneron, K. Brindle, E. Y. Chekmenev, A. Comment, C. H. Cunningham, R. J. DeBerardinis, G. G. Green, M. O. Leach, S. S. Rajan, R. R. Rizi, B. D. Ross, W. S. Warren and C. R. Malloy, *Neoplasia*, 2011, **13**, 81-97.
13. K. F. Bonhoeffer and P. Harteck, *Zeitschrift Fur Elektrochemie Und Angewandte Physikalische Chemie*, 1929, **35**, 621-623.
14. C. R. Bowers and D. P. Weitekamp, *Phys. Rev. Lett.*, 1986, **57**, 2645-2648.
15. C. R. Bowers and D. P. Weitekamp, *J. Am. Chem. Soc.*, 1987, **109**, 5541-5542.
16. M. G. Pravica and D. P. Weitekamp, *Chem. Phys. Lett.*, 1988, **145**, 255-258.
17. T. C. Eisenschmid, R. U. Kirss, P. P. Deutsch, S. I. Hommeltoft, R. Eisenberg, J. Bargon, R. G. Lawler and A. L. Balch, *J. Am. Chem. Soc.*, 1987, **109**, 8089-8091.
18. J. Bargon, J. Kandels and P. Kating, *J. Chem. Phys.*, 1993, **98**, 6150-6153.
19. S. B. Duckett, R. J. Mawby and M. G. Partridge, *Chem. Commun.*, 1996, 383-384.
20. A. Harthun, R. Kadyrov, R. Selke and J. Bargon, *Angewandte Chemie-International Edition in English*, 1997, **36**, 1103-1105.
21. D. Blazina, S. B. Duckett, P. J. Dyson and J. A. B. Lohmann, *Chemistry-a European Journal*, 2003, **9**, 1045-1061.
22. C. Deibele, A. B. Permin, V. S. Petrosyan and J. Bargon, *Eur. J. Inorg. Chem.*, 1998, 1915-1923.
23. J. Lopez-Serrano, S. B. Duckett, S. Aiken, K. Q. A. Lenero, E. Drent, J. P. Dunne, D. Konya and A. C. Whitwood, *J. Am. Chem. Soc.*, 2007, **129**, 6513-6527.
24. J. P. Dunne, S. Aiken, S. B. Duckett, D. Konya, K. Q. A. Lenero and E. Drent, *J. Am. Chem. Soc.*, 2004, **126**, 16708-16709.
25. J. Lopez-Serrano, S. B. Duckett, J. P. Dunne, C. Godard and A. C. Whitwood, *Dalton Trans.*, 2008, 4270-4281.
26. K. D. Atkinson, M. J. Cowley, S. B. Duckett, P. I. P. Elliott, G. G. R. Green, J. n. López-Serrano, I. G. Khazal and A. C. Whitwood, *Inorg. Chem.*, 2008, **48**, 663-670.
27. R. W. Adams, J. A. Aguilar, K. D. Atkinson, M. J. Cowley, P. I. P. Elliott, S. B. Duckett, G. G. R. Green, I. G. Khazal, J. López-Serrano and D. C. Williamson, *Science*, 2009, **323**, 1708-1711.
28. J. B. Hovener, N. Schwaderlapp, R. Borowiak, T. Lickert, S. B. Duckett, R. E. Mewis, R. W. Adams, M. J. Burns, L. A. R. Highton, G. G. R. Green, A. Olaru, J. Hennig and D. von Elverfeldtt, *Anal. Chem.*, 2014, **86**, 1767-1774.
29. H. Zeng, J. Xu, J. Gillen, M. T. McMahon, D. Artemov, J.-M. Tyburn, J. A. B. Lohman, R. E. Mewis, K. D. Atkinson, G. G. R. Green, S. B. Duckett and P. C. M. van Zijl, *Journal of Magnetic Resonance*, 2013, **237**, 73-78.
30. E. B. Duecker, L. T. Kuhn, K. Muennemann and C. Griesinger, *J. Magn. Reson.*, 2012, **214**, 159-165.
31. M. Fekete, O. W. Bayfield, S. B. Duckett, S. Hart, R. E. Mewis, N. Pridmore, P. J. Rayner and A. Whitwood, *Inorg. Chem.*, 2013, **52**, 13453-13461.
32. N. M. Zacharias, H. R. Chan, N. Sailasuta, B. D. Ross and P. Bhattacharya, *J. Am. Chem. Soc.*, 2012, **134**, 934-943.
33. R. V. Shchepin and E. Y. Chekmenev, *J. Labelled Compd. Radiopharm.*, 2013, **56**, 655-662.
34. F. Reineri, D. Santelia, A. Viale, E. Cerutti, L. Poggi, T. Tichy, S. S. D. Premkumar, R. Gobetto and S. Aime, *J. Am. Chem. Soc.*, 2010, **132**, 7186-7193.
35. R. Crabtree, *Acc. Chem. Res.*, 1979, **12**, 331-338.
36. R. H. Crabtree, H. Felkin and G. E. Morris, *J. Organomet. Chem.*, 1977, **141**, 205-215.
37. K. D. Atkinson, M. J. Cowley, P. I. P. Elliott, S. B. Duckett, G. G. R. Green, J. Lopez-Serrano and A. C. Whitwood, *J. Am. Chem. Soc.*, 2009, **131**, 13362-13368.
38. R. W. Adams, S. B. Duckett, R. A. Green, D. C. Williamson and G. G. Green, *J. Chem. Phys.*, 2009, **131**, 194505.
39. Q. X. Gong, A. Gordji-Nejad, B. Blumich and S. Appelt, *Anal. Chem.*, 2010, **82**, 7078-7082.
40. J.-B. Hövener, N. Schwaderlapp, T. Lickert, S. B. Duckett, R. E. Mewis, L. A. R. Highton, S. M. Kenny, G. G. R. Green, D. Leibfritz, J. G. Korvink, J. Hennig and D. von Elverfeldt, *Nat Commun*, 2013, **4**, doi:10.1038/ncomms3946.
41. K. V. Kovtunov, V. V. Zhivonitko, I. V. Skovpin, D. A. Barskiy and I. V. Koptyug, in *Hyperpolarization Methods in Nmr Spectroscopy*, ed. L. T. Kuhn, Springer-Verlag Berlin, Berlin, 2013, vol. 338, pp. 123-180.
42. L. S. Lloyd, R. W. Adams, M. Bernstein, S. Coombes, S. B. Duckett, G. G. R. Green, R. J. Lewis, R. E. Mewis and C. J. Sleigh, *J. Am. Chem. Soc.*, 2012, **134**, 12904-12907.
43. P. D. Morran, S. B. Duckett, P. R. Howe, J. E. McGrady, S. A. Colebrooke, R. Eisenberg, M. G. Partridge and J. A. B. Lohman, *J. Chem. Soc., Dalton Trans.*, 1999, 3949-3960.
44. B. Eguillor, P. J. Caldwell, M. C. R. Cockett, S. B. Duckett, R. O. John, J. M. Lynam, C. J. Sleigh and I. Wilson, *J. Am. Chem. Soc.*, 2012, **134**, 18257-18265.
45. J. Bargon, J. Kandels, P. Kating, A. Thomas and K. Woelk, *Tetrahedron Lett.*, 1990, **31**, 5721-5724.
46. R. Giernoth, H. Heinrich, N. J. Adams, R. J. Deeth, J. Bargon and J. M. Brown, *J. Am. Chem. Soc.*, 2000, **122**, 12381-12382.
47. M. J. Cowley, R. W. Adams, K. D. Atkinson, M. C. R. Cockett, S. B. Duckett, G. G. R. Green, J. A. B. Lohman, R. Kerssebaum, D. Kilgour and R. E. Mewis, *J. Am. Chem. Soc.*, 2011, **133**, 6134-6137.
48. B. J. A. van Weerdenburg, S. Gloggler, N. Eshuis, A. H. J. Engwerda, J. M. M. Smits, R. de Gelder, S. Appelt, S. S. Wymenga, M. Tessari, M. C. Feiters, B. Blumich and F. P. J. T. Rutjes, *Chem. Commun.*, 2013, **49**, 7388-7390.
49. H. Clavier and S. P. Nolan, *Chem. Commun.*, 2010, **46**, 841-861.
50. R. A. Kelly III, H. Clavier, S. Giudice, N. M. Scott, E. D. Stevens, J. Bordner, I. Samardjiev, C. D. Hoff, L. Cavallo and S. P. Nolan, *Organometallics*, 2007, **27**, 202-210.
51. C. A. Tolman, *Chemical Reviews*, 1977, **77**, 313-348.

52. O. Torres, M. Martín and E. Sola, *Organometallics*, 2009, **28**, 863-870.
53. C. Y. Tang, J. Lednik, D. Vidovic, A. L. Thompson and S. Aldridge, *Chem. Commun.*, 2011, **47**, 2523-2525.
54. O. Torres, M. Martin and E. Sola, *Organometallics*, 2009, **28**, 863-870.
55. D. G. Gusev, *Organometallics*, 2009, **28**, 6458-6461.
56. L. Pazderski, *Magn. Reson. Chem.*, 2008, **46**, S3-S15.
57. S. Wieland and R. Vaneldik, *Organometallics*, 1991, **10**, 3110-3114.
58. B. J. Coe and S. J. Glenwright, *Coord. Chem. Rev.*, 2000, **203**, 5-80.
59. P. Leoni, M. Sommovigo, M. Pasquali, S. Midollini, D. Braga and P. Sabatino, *Organometallics*, 1991, **10**, 1038-1044.
60. X. L. Luo, G. K. Schulte and R. H. Crabtree, *Inorg. Chem.*, 1990, **29**, 682-686.
61. R. H. Crabtree, G. G. Hlatky, C. P. Parnell, B. E. Segmuller and R. J. Uriarte, *Inorg. Chem.*, 1984, **23**, 354-358.
62. J. M. Brown, *Chem. Soc. Rev.*, 1993, **22**, 25-41.
63. A. B. Permin and R. Eisenberg, *J. Am. Chem. Soc.*, 2002, **124**, 12406-12407.
64. D. J. Fox, S. B. Duckett, C. Flaschenriem, W. W. Brennessel, J. Schneider, A. Gunay and R. Eisenberg, *Inorganic Chemistry*, 2006, **45**, 7197-7209.
65. M. Fekete, O. Bayfield, S. B. Duckett, S. Hart, R. E. Mewis, N. Pridmore, P. J. Rayner and A. Whitwood, *Inorganic Chemistry*, 2013.
66. D. A. Barskiy, K. V. Kovtunov, I. V. Koptyug, P. He, K. A. Groome, Q. A. Best, F. Shi, B. M. Goodson, R. V. Shchepin, A. M. Coffey, K. W. Waddell and E. Y. Chekmenev, *J. Am. Chem. Soc.*, 2014, **136**, 3322-3325.
67. N. Eshuis, N. Hermkens, B. J. A. van Weerdenburg, M. C. Feiters, F. Rutjes, S. S. Wijmenga and M. Tessari, *J. Am. Chem. Soc.*, 2014, **136**, 2695-2698.
68. S. Gloggler, M. Emondts, J. Colell, R. Muller, B. Blumich and S. Appelt, *Analyst*, 2011, **136**, 1566-1568.